Dynamics-level Design for Discrete- and Continuous-Time Band-pass Sigma-Delta-Modulators for Micro-machined Accelerometers

Luo, J. Rapisarda, P. Kraft, M.

Abstract— **High-performance micro-electro-mechanical systems (MEMS) sensors can be implemented by incorporating a micro-machined capacitive sensing element in a Sigma-Delta-Modulators ($\Sigma\Delta M$) force-feedback loop, forming an electro-mechanical $\Sigma\Delta M$ ($EM-\Sigma\Delta M$). We propose a transfer-function based design methodology to realize discrete- and continuous-time low-pass electro-mechanical $\Sigma\Delta M$ systems. The design is performed at the level of the integrated system consisting of the electro-mechanical sensor and of the electronic circuit; we call this the *dynamics-level*. We also illustrate a technique to perform the conversion of the discrete-time design to a continuous-time one. The approach is demonstrated through an electro-mechanical $\Sigma\Delta M$ design example for a bulk micro-machined, capacitive accelerometer.**

I. Introduction

Micro-machined accelerometers are widely used in air-bag systems in vehicles, in vibration measurement, in inertial guidance, and many other applications. Most modern micro-machined sensing elements consist of a proof mass which is deflected due to the inertial force, resulting in a differential capacitive signal which is then amplified. Since the differential changes in the capacitive signal are very small, a high-resolution interface circuit becomes of primary importance in design. Equally important is the incorporation of the sensing element in a force-feedback control scheme so as to increase the linearity, dynamic range and bandwidth of the sensor, and to reduce sensitivity to fabrication imperfections and susceptibility to environmental parameter changes. Compared to analogue force feedback control strategies, closed-loop force-feedback control schemes based on Sigma-Delta modulators ($\Sigma\Delta M$ in the following) have many advantages [1]; in particular, they produce a direct digital output which can be directly processed further by a digital signal processor. In such a scheme, the micromachined sensing element is part of the control loop to form an *electro-mechanical* $\Sigma\Delta M$. The design problem is to determine parameters for the control loop that guarantee the stability of the overall system and a good performance in terms of signal-to-noise ratio.

Initially, in order to design electro-mechanical $\Sigma\Delta M$ standard approaches developed in the context of purely electronic $\Sigma\Delta M$ analog-digital convertors (ADC) were used, see [2], [3]. However, electro-mechanical $\Sigma\Delta M$ are fundamentally different from purely electronic ones, since integrating the micro-machined sensing element without losing loop stability and performance introduces additional difficulties in the design. Since there is no exact theoretical analysis method due to the non-linearity of the quantizer, and since fabrication tolerances and environmental conditions introduce uncertainties, designs are often validated through system level simulations. This approach is rather inefficient, since a large number of different scenarios must be simulated and analyzed before sufficient confidence can be established to adopt a given design. Moreover, often the optimization of the parameters is performed directly on a specific circuit chosen for the implementation, and the resulting designs are topology-dependent.

Recently in [4], [5], an 'unconstrained architecture' (also called topology in the following) has been proposed for the case of a MEMS gyroscope. The topology is called "unconstrained" since it has the necessary degrees of freedom to accommodate an arbitrary second order dynamical model. This approach constitutes a major inspiration for the results presented in this paper; we briefly review its salient features. In [4], [5], the need for system-level simulations is significantly reduced by the adoption of a "filter-level" design, of an elegant analytical framework, and of a set of clear-cut design guidelines. The methodology is developed essentially for a second-order model for the sensing element, and for a specific system topology; this makes the mapping between the designed QNTF to the circuit rather straightforward. However, the adoption of higher-order models (often necessary to model the complex dynamics of the sensing element) requires using different topologies, which are not presented in [5]. Another aspect not discussed explicitly in [5] is the conversion of the design from discrete- to continuous-time.

In this paper we address both these issues. We distinguish three phases in the design of $\Sigma\Delta M$, namely:

- *dynamics-level design*: designing the QNTF and the signal transfer function at the system-level, i.e. with the sensing element integrated in the loop filter;
- *topology-level design*: synthesizing the loop filter into a desired circuit topology;
- *circuit-level design*: circuit behavior and layout design.

We concentrate on dynamics-level design, taking as starting point the work illustrated in [6]; standard techniques for design at the topology- and circuit-level for purely electronic $\Sigma\Delta M$ (see for example [7], [8], [9], [10], [11]) can be used for the other two phases. This approach entails two advantages. Firstly there is the decoupling of design (performed in the first phase) and implementation (performed in the last two phases and aimed at solving issues specific to

J. Luo, P. Rapisarda, H. Ding and M. Kraft are with the School of Electronics and Computer Science, University of Southampton, Southampton, UK. SO17 1BJ.
E-mail: luoj@soton.ac.uk, pr3@ecs.soton.ac.uk and mk1@ecs.soton.ac.uk

ISBN 978-963-311-370-7

the application). Secondly, in the design phase it is easy to accommodate higher-order models for the sensing element given that the computations are transfer-function based.

At the dynamics level, we design the QNTF of a discrete-time $\Sigma\Delta M$ under constraints that specifically model the integration of the sensing element in the system, as in the approach of [5], [12]. After converting the QNTF into an open-loop filter, the splitting of the sensing element and the electronic part of this filter is carried out. In this phase we only use transfer function manipulations, without restricting ourselves to an a priori specified topology.

In this paper we also consider the problem of how to convert a discrete-time design to an 'equivalent' continuous-time one at the dynamics-level. A direct conversion does not preserve the separation of the mechanical and the electronic part; consequently, we introduce a mixed-feedback topology including a signal- and a compensation path in order to accommodate the dynamics of the sensing element, and then convert separately the resulting transfer functions to continuous-time through standard techniques.

This paper is organized as follows. In section II, a system-level analysis is carried out for the discrete-time case to establish a relationship between the quantization noise transfer function and the *open-loop system transfer function*. We proceed to illustrate our design procedure and to exemplify it with a fourth-order example. In section III, the conversion from a discrete-time electro-mechanical $\Sigma\Delta M$ design to an equivalent continuous-time system is discussed. In the final section of the paper, conclusions are drawn and some current and future research work is outlined.

II. TRANSFER-FUNCTION-BASED DISCRETE-TIME DESIGN

In this section we present a design procedure for single-loop EM-$\Sigma\Delta M$ systems, which are often chosen for electromechanical applications (see [2]) due to their high tolerance to parameters variations.

A. System analysis of single-loop electro-mechanical $\Sigma\Delta M$

A simplified single-feedback electro-mechanical $\Sigma\Delta M$ is shown in Fig. 1, including the sensing element with transfer function $G_s(s)$, the electronic interface and filter circuit part with transfer function $H_c(s)$, the feedback-force block k_{fb} and the quantizer.

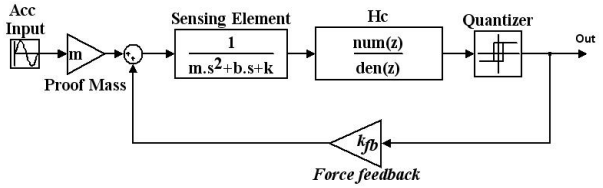

Fig. 1. Block diagram of electro-mechanical $\Sigma\Delta M$ system

This simplified model neglects several factors affecting the dynamics of a real-world electro-mechanical system, for example nonlinearities arising from non-ideal components, from additional electrostatic force components, and from the feedback voltage to electro-static force conversion; and non-constant damping and spring coefficients. However, in the simulations used for validating the design technique proposed in this paper we do consider several of these non-ideal effects. It is also important to note that although the the sensor element G_s in Fig. 1 is described by a second-order transfer function, our methodology can be used without modifications for higher-order models.

In the second-order case the dynamics of the sensing element are described in continuous-time as:

$$G_s(s) = \frac{1}{ms^2 + bs + k} \,, \tag{1}$$

where m is the proof mass (measured in Kg), b is the damping coefficient (measured in $N/m/s$), and k is the stiffness constant (measured in N/m). As shown in [5], assuming a zeroth order DAC, the transfer function (1) has a discrete-time domain equivalent

$$G_s(z) = k_s \frac{z - b_s}{(z - a_s)(z - a_s^*)} \,, \tag{2}$$

for suitable values of the constants a_s (computed from the continuous-time poles of (1) via the usual continuous-to-discrete-time mapping formula), k_s, and b_s. Of particular relevance for the following is the presence in (2) of the zero b_s, which is absent in the continuous-time model.

Quasi-linear models have proved to be effective in dealing with the nonlinearity of $\Sigma\Delta M$ in many successfully $\Sigma\Delta M$ applications, see [13], [1], [5]. In these models the nonlinearity of the one-bit quantizer is replaced with a gain k_q and a quantisation error e_Q (see section III of [14]). Consequently, a linearized model for the discrete-time QNTF, denoted with QNTF(z), can be written as:

$$QNTF(z) = \frac{1}{1 - G_s(z)H_c(z)k_q k_{fb}} \,. \tag{3}$$

In the following we consider the *open-loop system transfer function* $G_O(z) := G_s(z)H_c(z)k_q k_{fb}$ which we can factorize as $G_O(z) =: \frac{B_O(z)}{A_O(z)}$, with B_O and A_O defined by

$$k_O \frac{(z - b_s)(z - b_{O,2}) \ldots (z - b_{O,n_{Ob}})}{(z - a_s)(z - a_s^*)(z - a_{O,3}) \ldots (z - a_{O,n_{Oa}})} \,. \tag{4}$$

Analogously, $QNTF(z)$ is factorized as

$$QNTF(z) =: \frac{B_N(z)}{A_N(z)} = k_N \frac{(z - b_{N,1}) \ldots (z - b_{N,n_{Nb}})}{(z - a_{N,1}) \ldots (z - a_{N,n_{Na}})} \,. \tag{5}$$

It is a matter of straightforward verification to check that from (3) and from $G_O(z) = G_s(z)H_c(z)k_q k_{fb}$ it follows that

$$G_O(z) = \frac{1 - QNTF(z)}{QNTF(z)} = \frac{B_O(z)}{A_O(z)} = \frac{A_N(z) - B_N(z)}{B_N(z)}. \tag{6}$$

B. Constraints for QNTF design in EM-$\Sigma\Delta M$

It is a matter of straightforward calculations to show that since the open loop dynamics (4) contains the zero b_s of the sensing element, then $G_o(b_s) = 0$ and $QNTF(b_s) = 1$. Consequently, the QNTF in a n-th order force-feedback electro-mechanical $\Sigma\Delta M$ system has the following form:

$$QNTF(z) = \frac{(z-a_s)(z-a_s^*)(z-b_{N,3})\dots(z-b_{N,n})}{(z-a_{N,1})\dots(z-a_{N,n})} \tag{7}$$

A third constraint arises from an empirical criterion (see [13]) used to ensure the stability of the closed-loop transfer function, namely $\|QNTF\|_\infty < 2.0$. (When the system order is higher than 5, it is suggested that $\|QNTF\|_\infty < 1.5$ (see [1]).) The fourth constraint is the stability of the QNTF.

Summarizing, the following constraints must be satisfied:

1) $QNTF(b_s) = 1$;
2) $QNTF(z)$ is of the form as eq. (7);
3) $|QNTF(z)|_\infty < g_{max}$, where $g_{max} = 2.0$ or 1.5;
4) All poles of $QNTF(z)$ are in $\{z \in \mathbb{C} \mid |z| < 1\}$.

C. Simplify QNTF design through open loop manipulation

In a single-feedback scheme the signal transfer function is completely determined by the QNTF; consequently a standard design heuristic is that a 'good' QNTF also leads to a 'good' QSNR, see [1]. The first stage in our procedure is to design a realizable high-pass QNTF filter to achieve the desired noise shaping performance, while satisfying the constraints $1)-4)$ stated at the end of subsection II-B. This step involves solving a mathematical optimization problem in the $2n-2$ decision variables $b_{N,3},\dots,b_{N,n}$, $a_{N,1},\dots,a_{N,n}$ appearing in 7, under the constraints $1)-4)$ of section II-B. This is a non-convex problem, difficult to solve analytically and computationally intensive to tackle using numerical methods (see [15], [7] for an exploration algorithm); in this article we concentrate on achieving a sub-optimal solution.

The problem of designing the QNTF can be simplified by releasing the equality constraint $1)$. In [5], this is done with the 'unconstrained architecture', through the introduction of a mixed-feedback scheme. In our design method, we use the following equivalent conversion with the open loop dynamics. Considering a QNTF of the form (7), we obtain

$$G_o(z) = k_O \frac{(z-b_{O,1})\dots(z-b_{O,n_{Ob}})}{(z-a_s)(z-a_s^*)(z-b_{N,3})\dots(z-b_{N,n})}, \tag{8}$$

where $n_{Ob} < n$. We then introduce a fictitious zero-pole pair (b_s, b_s) in 8 as follows:

$$\begin{aligned} G'_O(z) &= k_s \frac{z-b_s}{(z-a_{s1})(z-a_{s2})} \cdot \frac{k_O}{k_s k_q k_{fb}} \\ &\quad \cdot \frac{(z-b_{O,1})\dots(z-b_{O,n_{Ob}})}{(z-b_s)(z-b_{N,3})\dots(z-b_{N,n})} \cdot k_q k_{fb} \\ &=: G_s(z)\cdot k'_O \\ &\quad \cdot \frac{(z-b_{O,1})\dots(z-b_{O,n_{Ob}})}{(z-b_s)(z-b_{N,3})\dots(z-b_{N,n})} \cdot k_q k_{fb} \end{aligned} \tag{9}$$

where k_q can be considered as 1 at the dynamics-level design stage, since an arbitrary open loop gain can be cascaded before quantizer without affecting QSNR performance, see [1], [16]. This open loop dynamics is of the form $G_s(z)H'_c(z)k_{fb}$, with

$$H'_c(z) := k'_O \frac{(z-b_{O,1})\dots(z-b_{O,n-1})}{(z-b_s)(z-b_{N,3})\dots(z-b_{N,n})} \tag{10}$$

being the *nominal circuit filter*. We now proceed to design the QNTF under the constraints $2)-4)$ of sect. II-B.

D. Design methodology for discrete-time $EM-\Sigma\Delta M$

We formalise our procedure in the flow-chart in Fig. 2. Major steps in the procedure are represented by solid boxes; their execution is split up in the series of actions described in the dashed-border boxes. These detailed steps can be performed in several ways, which may involve iterations and trade-offs achieved by rule-of-thumb; these will be described in the design example in section II-E.

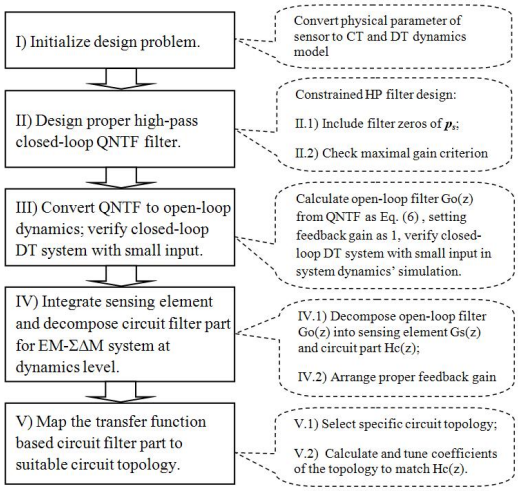

Fig. 2. Design procedure for discrete-time low-pass $EM-\Sigma\Delta M$

(I) Obtain CT and DT dynamics model from the sensor's parameters, including its poles and zeros.

(II) This is a constrained linear filter design that can be solved in many ways. In [5] the authors propose an effective solution to arrange QNTF's poles and zeros based on some results of [12], [1]. We use a technique developed for purely electrical $\Sigma\Delta M$, see Appendix V and the design example below.

(III) Use eq. (6) to compute the open-loop dynamics $G_o(z)$ from the designed QNTF. At this stage we are only concerned with the location of the poles and the zeroes, and only with the sign of the gains of the transfer functions. The value of the gains are not important, although of course they affect stability greatly and need to be chosen carefully later on. In the following we call a representation of a transfer function with gain ± 1 a *normalized zpk* (zero-pole-gain) *representation*.

The DT $\Sigma\Delta M$'s open-loop dynamics comprises the $G_o(z)$ computed above and the quantizer; its stability

can be verified in simulations by inserting small signal input after quantizer.

(IV) Various choices can be effected. In [5] an unconstrained topology ('architecture') based on a mixed-feedback is proposed at the topology level. We integrate the sensing element through transfer function manipulation at the dynamics-level, by integrating the constraint regarding the sensing element's poles in QNTF design and introducing a fictitious zero-pole pair (b_s, b_s) in the conversion to open loop dynamics, see (5) and (9).
The second important issue to address in this step is to decide the value of feedback gain k_{fb}. For a single-feedback scheme, it is important to ensure that $K_{\max}\|\mathbf{input}\| < \|\mathbf{feedback}\|$ is satisfied (see [13]), where **input** is the input force, **feedback** is the feedback force, and $K_{\max}$ is an empirical threshold.

(V) The problem of realizing a nominal circuit filter $H_c'(z)$ with an optimized topology has been well studied in purely electrical $\Sigma\Delta M$ design, see [8], [10]. In this step practical issues, e.g. circuit complexity, coefficient sensitivity and power consumption can addressed.

E. Design example: fourth-order low-pass $\Sigma\Delta M$ for a MEMS accelerometer

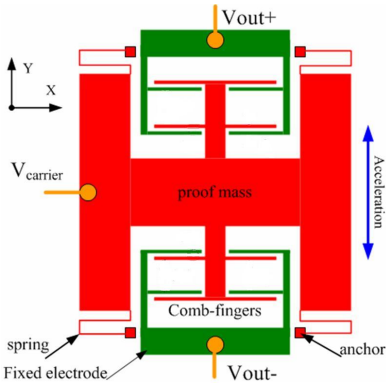

Fig. 3. Schematic diagram of a capacitive accelerometer [16]

We use the high-performance capacitive accelerometer schematically shown in Fig. 3, considered also in [17], [18], [16]. The lumped parameters of the bulk-micro-machined accelerometer sensing element are summarized in Table I. We follow the procedure schematised in Fig. 2:

Mass of proof mass	m (kg)	1.2×10^{-6}
Damping coefficients	b $(N/m \cdot s)$	6.0×10^{-3}
Spring stiffness	k (N/m)	5.0
Resonant frequency	(Hz)	325
Quality factor		0.41
Static sensitivity	(pF/g)	16.5
Static sensing capacitance	(pF)	21.03
Sensing gap distance	(μm)	3
Maximal acceleration	G_{max} (G)	$\pm$ 1

TABLE I
LUMPED PARAMETERS OF THE ACCELEROMETER [16], [17]

(I): We assume that the sampling frequency $f_s = 131072$Hz, and that the bandwidth $f_{bw} = 1024$Hz. Consequently $G_s(z) = 2.397 \times 10^{-5} \frac{(z+0.988)}{(z-0.992)(z-0.971)}$ with one zero as $b_s = -0.987$, and two poles as $\{a_s, a_s^*\} = \{0.992, 0.970\}$.

(II): The poles of the sensing element $\{a_s, a_s^*\} = \{0.992, 0.970\}$; using the heuristic described in Appendix V, we choose the remaining zeroes through the optimal arrangement of zeros for a second order purely electrical $\Sigma\Delta M$ as $e^{\pm j0.5774\phi_1} = \{0.9996 \pm 0.02834j\}, \phi_1 = \frac{f_{bw}}{fs} \cdot 2\pi$. Finally, the poles of QNTF are determined with inverse Chebyshev functions as described in Appendix V: four poles are selected as in a fourth order 'E1' scheme from Table 4.4 in [13], i.e., $\{0.78391 \pm 0.3333j, 0.6570 \pm 0.1157j\}$. The Bode plot of the designed $QNTF$

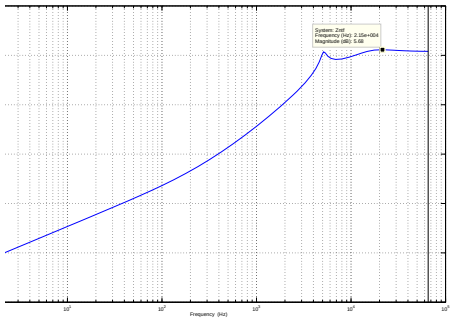

Fig. 4. Bode plot of QNTF

in Fig. 4 shows that $\|QNTF(z)\|_\infty = 4.76$dB $= 1.730 < g_{\max} = 2$.

(III): The open-loop transfer function $G_o(z)$ is computed according to (6):

$$-\frac{(z-0.7623)(z^2-1.697z+0.7772)}{(z-0.992)(z-0.9704)(z^2-1.999z+1)}. \quad (11)$$

(IV): The decomposition of $G_s(z)$ as in 9 and 10 yields

$$H_c'(z) = -\frac{(z-0.762)(z^2-1.697z+0.777)}{(z+0.987)(z^2-1.999z+1)}$$

We now need to set the feedback force gain k_{fb} and the circuit gain k_c. Considering the electronic noise from front-end amplifier, k_{fb} is set as $k_{fb} = 1.22 \times 10^{-5}$ in system-level simulations.

(V): We use the classical cascaded scheme based on biquad configuration [11] to map the designed transfer function to a circuit.

We now validate the design obtained with the `Matlab Simulink` model depicted in Fig. 6. There are some differences with respect to Fig. 1: firstly, the feedback force gain is implemented through a force-feedback linearization scheme with feedback voltage $V_{fb} = 6.5\ V$, as discussed in [18]. Moreover, $H_c'(z)$ is implemented in a biquad configuration

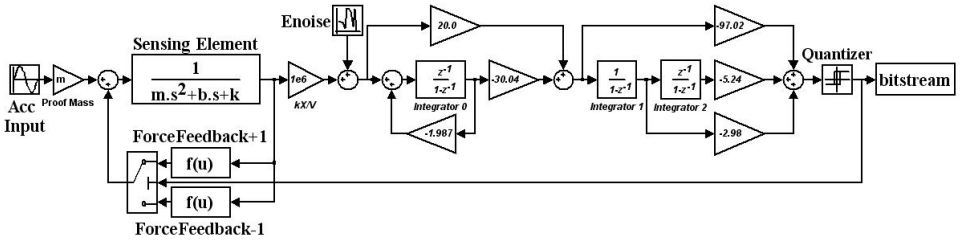

Fig. 5. Realization of 4th order discrete-time electro-mechanical $\Sigma\Delta M$

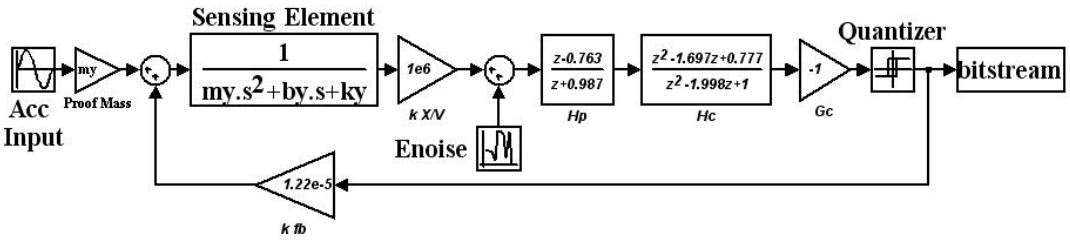

Fig. 6. `Simulink` model of fourth order discrete-time electro-mechanical $\Sigma\Delta M$

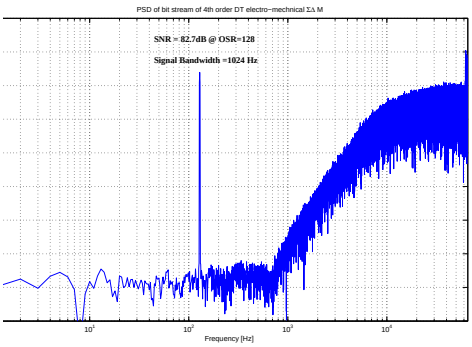

Fig. 7. PSD of output bitstream of the 4th order DT electro-mechanical $\Sigma\Delta M$

(see Chapter 9 of [19]) with $H_{d_1}(z)$ and $H_{d_2}(z)$ as in Fig. 5. The circuit topology diagram is shown in Fig. 5.

In simulations we chose the acceleration input signal $x(t) = 0.5\ G \cdot sin(2\pi f_{in} t)$ to avoid overloading, where $f_{in} = 128\ Hz$. The oversampling ratio is $ORS = 128$, and the signal bandwidth is $f_{bw} = 1024$Hz, so that the sampling frequency is $f_s = 131072\ Hz$. We placed an input-referred white-noise source (the '`Enoise`' module in Fig. 6) with a realistic power spectral density (PSD) equal to 6 $\frac{nV}{\sqrt{Hz}}$ at the input of the pick-off amplifier (see [20]).

In simulations, the system in Fig. 6 achieves an $82.7dB$ SQNR, as shown in Fig. 7. Comparing this result to the $82\ dB$ value obtained for the same MEMS accelerometer in [17], shows that our design method directly produces a fourth-order electro-mechanical $\Sigma\Delta M$ system with competitive performance without the need for any time-consuming system-level simulation.

Remark 1: It has been confirmed in simulations that our design performs well also when the parameters of the second-order model in 1 are changed considerably, even up to unrealistic values.

III. Discrete- to continuous-time $\Sigma\Delta M$ conversion

EM-$\Sigma\Delta M$ are often based on discrete-time circuits; however, discrete implementations also have disadvantages which may suggest considering a continuous implementation. However, design for continuous-time EM-$\Sigma\Delta M$ is not straightforward: while the quasi-linear model is a reasonable approximation in the discrete-time case, this assumption is not applicable in the continuous-time case. It is because of this that the need for the conversion of discrete- to continuous-time designs arises.

A. Discrete- to continuous-time conversion via the equivalent closed-loop impulse response

In the purely electronic $\Sigma\Delta M$ domain, a widely used method for the conversion of discrete-time systems to continuous-time is the *equivalent impulse response* (see [21], [22]); this technique has also been partially used in the context of electro-mechanical $\Sigma\Delta M$ in [17], [18]. The basic idea of this method is illustrated in Figure 8: the discrete-time system transfer function $G_o(z)$ is substituted by an "equivalent" continuous-time transfer function $G_o(s)$ preceded by a digital-to-analog converter (DAC) and followed by a sampler with sampling frequency f_s. $G_o(s)$ is chosen so that the values of the discrete-time signal $x_d(\cdot)$ on the left-hand side of Figure 8 and of the sampled version $x'_d(\cdot)$ of the continuous-time signal $x_c(\cdot)$ on the right-hand side of the figure are equal at the sampling instants. In the following discussion we consider a None-Return (Zero-Order-Hold)

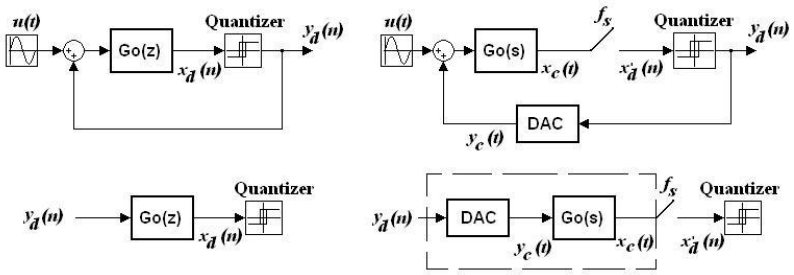

Fig. 8. Conversion from discrete- to continuous-time $\Sigma\Delta M$

DAC scheme, since it is the most widely used in various applications.

B. Decomposition of sensing element and circuit filter in dynamics-level

Following the assumption and discussion in section II, without losing generality, we can assume that the result of the conversion from the DT open loop dynamics in 4 is

$$\begin{aligned} G_o(s) &= \frac{B_o(s)}{A_o(s)} \\ &= \frac{k_O^c(s-b_{O,1}^c)\dots(s-b_{O,n_{Oa}-1}^c)}{(s-a_{s1}^c)(s-a_{s2}^c)(s-a_{O,3}^c)\dots(s-a_{O,n_{Oa}}^c)}, \end{aligned} \tag{12}$$

where $\{a_{s1}^c, a_{s2}^c\}$ represent two poles of the second order model sensing element, k_O^c is the nominal gain, n_{Oa} is the order of open loop dynamics, $\{a_{O,i}^c, i=3,\dots,n_{Oa}-1\}$ are poles of open loop dynamics except $\{a_{s1}^c, a_{s2}^c\}$, and $\{b_{O,i}^c, i=1,\dots,n_{Oa}-1\}$ the zeros of open loop dynamics.

In general it is not guaranteed that $\deg(B_o(s)) < \deg(A_o(s))-1$; moreover, the presence of the sensing element $G_s(s)=\frac{k_s^c}{(s-a_{s1}^c)(s-a_{s2}^c)}$ requires that the numerator has degree equal to $(\deg(A_o(s))-2)$. Therefore, direct decomposition by cascading the sensing element with the circuit filter leads to an unrealisable filter.

In order to decompose the open loop dynamics $G_o(s)$, we preserve the separation of mechanical and electronic dynamics based on the mixed-feedback scheme shown in Fig. 9. Two paths are present: the *signal path* integrating the sensing element $G_s(s)$ and cascading part of the electronic circuit transfer function $H_{c_1}(s)$; and the *compensation path* containing another part of circuit filter $H_{c_2}(s)$ to compensate the difference of the impulse response between after CT *signal path* and before the quantizer in DT $\Sigma\Delta M$. In transfer functions terms, given $G_s(s)$ as in (1) and $G_o(s)$ as in (12), there always exist proper rational functions $H_{c_1}(s)$ and $H_{c_2}(s)$ such that

$$G_o(s) = G_s(s)H_{c_1}(s) + H_{c_2}(s)\ . \tag{13}$$

It should be noted that the decomposition (13) is not unique. We propose the following decomposition approach.

1) Divide $B_o(s)$ by $(s-a_{s1}^c)(s-a_{s2}^c)$, obtaining $B_o(s)=(s-a_{s1}^c)(s-a_{s2}^c)B_O^*(s)+B_O^r(s)$, where $\deg(B_O^*(s))=(n_{Oa}-3)$, and $B_O^r(s)$ is the remainder, $\deg(B1_O^r(s))\le 1$.
2) Choose a polynomial $B1_O^*(s)$ with $\deg(B1_O^*(s)) \le (n_{Oa}-4)$;
3) Decompose $G_o(s)=\frac{B_o(s)}{A_o(s)}$ as:

$$\begin{aligned} & G_s(s)\frac{\frac{1}{k_s^c}((s-a_{s1}^c)(s-a_{s2}^c)B1_O^*(s)+B_O^r(s))}{(s-a_{O,3}^c)\dots(s-a_{O,n_{Oa}}^c)} \\ + \quad & \frac{B_O^*(s)-B1_O^*(s)}{(s-a_{O,3}^c)\dots(s-a_{O,n_{Oa}}^c)}; \end{aligned} \tag{14}$$

Now define the two transfer functions $H_{c_1}(s) := \frac{B_{c1}(s)}{A_{c1}(s)} = \frac{\frac{1}{k_s^c}((s-a_{s1}^c)(s-a_{s2}^c)B1_O^*(s)+B_O^r(s))}{(s-a_{O,3}^c)\dots(s-a_{O,n_{Oa}}^c)}$ and $H_{c_2}(s) := \frac{B_{c2}(s)}{A_{c2}(s)} = \frac{B_O^*(s)-B1_O^*(s)}{(s-a_{O,3}^c)\dots(s-a_{O,n_{Oa}}^c)}$. Observe that $\deg(B_{c1}(s)) \le (n_{Oa}-2) = \deg(A_{c1}(s))$ and $\deg(B_{c2}(s)) \le (n_{Oa}-2) = \deg(A_{c2}(s))$, and consequently $H_{c_1}(s)$ and $H_{c_2}(s)$ are proper rational functions which can be realized by circuits.

According to eq. (13), the choice of different $B1_O^*(s)$ does not affect equivalence between DT and CT open-loop dynamics, i.e., SQNR performance of $\Sigma\Delta M$. Theoretically, an arbitrary $B1_O^*(s)$ can be selected by designers to make a successful decomposition to complete dynamics-level design aiming at SQNR performance. In design practise, iterative searching of a suitable $B1_O^*(s)$ may be required to produce specific Signal Transfer Function (STF) when considering other requirements, such as, input noise along signal path.

Remark 2: In single-loop $\Sigma\Delta M$ the nominal circuit transfer function can have an arbitrary gain placed before the quantizer, whose value does not alter the performance of the system. When using a signal- and a compensation-path, their gains can be arbitrary, but they must be proportional to each other according to a fixed ratio.

C. Design methodology for continuous time EM-$\Sigma\Delta M$

Using the decomposition approach sketched above, the following design methodology for CT $EM-\Sigma\Delta M$ is obtained:

(I) Design open loop dynamics $G_o(z)$ for a DT $EM-\Sigma\Delta M$ as in steps I)-III) of Fig. 2;
(II) Convert CT open loop dynamics $G_o(z)$ to DT open loop dynamics $G_o(s)$ with preferred DAC;
(III) Decompose $G_o(s)$ as in (14) and realise the $EM-\Sigma\Delta M$ at dynamics level;
(IV) Map the open loop filter $H_{c1}(s)$ and $H_{c2}(s)$ to proper circuit topologies.

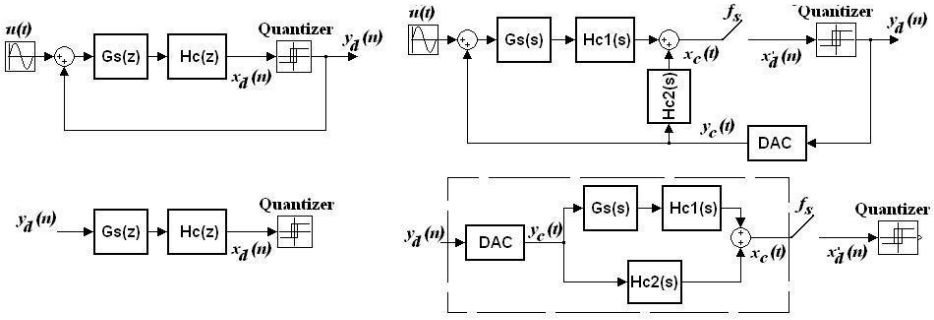

Fig. 9. Conversion from discrete- to continuous-time $\Sigma\Delta M$ with distributed feedback

We conclude this section with an example converting the design of section II-E to continuous-time.

D. Discrete- to continuous-time design conversion example

Step I is completed in design example in section II-E, obtaining $G_o(z)$ as in (11). Step II can be performed using the `Matlab` command `d2c` to convert $G_o(z)$ to CT open-loop dynamics, which yields following normalized zpk presentation $\overline{G}_o(s)$:

$$-\frac{(s+3.543\times10^4)(s^2+3.322\times10^4 s+1.572\times10^9)}{(s+3943)(s+1057)(s^2+1.38\times10^7)} \quad (15)$$

In step III, let $B1^*_O(s)=3\times10^4$; we decompose $G_o(s)$ as

$$\begin{aligned} G_o(s) &= \frac{8.33\times10^5}{s^2+5000s+4.167\times10^6}\cdot 0.036 \\ &\quad \cdot\frac{-(s^2+8.59\times10^4 s+1.85\times10^9)}{s^2+1.38\times10^7} \\ &\quad + \frac{-(s+3.37\times10^4)}{s^2+1.38\times10^7} \\ &= G_s(s)\cdot 0.036\cdot \overline{H}_{c_1}(s)+\overline{H}_{c_2}(s) \end{aligned} \quad (16)$$

where $\overline{H}_{c_1}(s)$ and $\overline{H}_{c_2}(s)$ are the normalized zpk representations of the signal path and compensation path transfer functions.

As mentioned in Remark 2, the signal path gain and the compensation path gain may vary, but they must have the same sign as $\overline{H}_{c_1}(s)$ and $\overline{H}_{c_2}(s)$, and a fixed ratio of 0.036. Through dynamics level simulation, we set $k_{fb}=4.6\times10^{-6}$ so as to tolerate electronic noise from the front-end amplifier, which has corresponding feedback voltage as $V_{fb}=4.0V$. The compensation path gain is set as 127.8.

In step IV, the distributed feedback and feed-forward topology, see[18], is adopted to map the designed filter to circuit topology.

In order to validate this design, we simulate the designed topology in `Matlab Simulink` with the model illustrated in Figure. 10. The converted continuous-time electro-mechanical $\Sigma\Delta M$ system achieves a SQNR of 86.0dB.

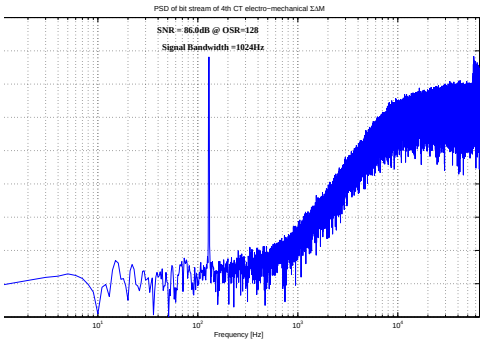

Fig. 11. PSD of output bitstream of the 4th order continuous-time electro-mechanical $\Sigma\Delta M$

IV. Conclusions

In this paper, we illustrated a three-stage design procedure for EM-$\Sigma\Delta M$ design, and we concentrated on the dynamics-level design. A complete dynamics-level design method was developed for DT and CT EM-$\Sigma\Delta M$. Design examples based on a high-performance accelerometer have been used to illustrate the design procedure. System-level simulations show that our designs are competitive when compared with previous work.

This paper presents only a basic concept to design EM-$\Sigma\Delta M$, on which further research is being carried out in several directions. Firstly, we plan to apply the methodology illustrated here to the case of higher-order $\Sigma\Delta M$ applications with more complex sensing element dynamics, in order to further validate our approach. Secondly, we want to investigate the possibility of setting up a mathematical optimization problem for the determination of the QNTF poles, and of finding efficient methods for its solution. Finally, we aim at incorporating uncertainty considerations in the design and at assessing in a systematic way the robustness of the electronic circuit in the face of parameter uncertainties.

V. Appendix

Design QNTF for EM-$\Sigma\Delta M$: This appendix describes the QNTF design method used to find suitable zeros and poles

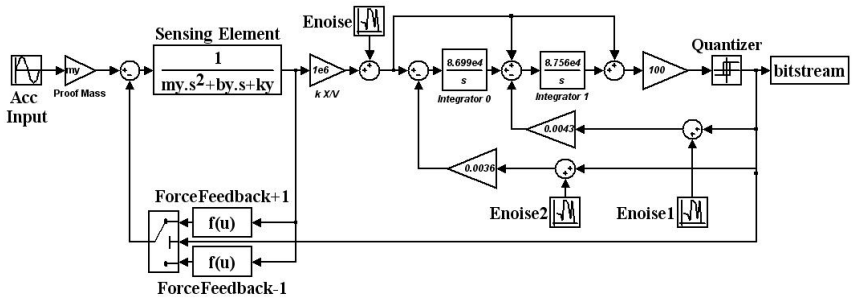

Fig. 10. Circuit realization of fourth order continuous-time electro-mechanical $\Sigma\Delta M$

for QNTF of EM-$\Sigma\Delta M$. Note that the arrangement of zeros and poles of QNTF is based on the quasi-linear model for $\Sigma\Delta M$, which is only approximate to the nonlinear dynamics of real $\Sigma\Delta M$. Consequently ours is not a strictly optimal solution but a sub-optimal one based on some empirical guidelines.

We first consider the zeros of QNTF in EM-$\Sigma\Delta M$ which dominate the in band quantisation noise. Given second order dynamics model for the sensing element in n-th order EM-$\Sigma\Delta M$, there are $n-2$ zeros of QNTF to determine. It is straightforward to use a zeros arrangement scheme for $(n-2)$-th QNTF as in purely electrical $\Sigma\Delta M$, see Table 4.1 in [1]. Secondly, the placement of the poles of the $\Sigma\Delta M$ has to be considered as a trade off between SQNR performance and system stability. Considering that the poles of the sensing element are different from the optimal zeros for purely electrical $\Sigma\Delta M$, we choose a relatively conservative scheme to arrage n poles using roots of Inverse Chebyshev functions as described in Chapter 4.6.2 of [13], see Table 4.4 in [13].

REFERENCES

[1] S. Norsworth, R. Schreier, and C. Temes, *Delta-Sigma Data Converters, Theory, Design, and Simulation*. Piscataway, NJ: IEEE Press, 1997.

[2] V. Petkov and B. Boser, "A fourth-order $\Sigma\Delta$ interface for micromachined inertial sensors," *Solid-State Circuits, IEEE Journal of*, vol. 40, no. 8, pp. 1602 – 1609, Aug. 2005.

[3] C. Lu, M. Lemkin, and B. Boser, "A monolithic surface micromachined accelerometer with digital output," *Solid-State Circuits, IEEE Journal of*, vol. 30, no. 12, pp. 1367 – 1373, Dec. 1995.

[4] J. Raman, E. Cretu, P. Rombouts, and L. Weyten, "A digitally controlled MEMS gyroscope with unconstrained Sigma-Delta force-feedback architecture," in *Proc. 19 th IEEE Int. Conf. on MEMS*, Jan. 2006, pp. 710–713.

[5] J. Raman, P. Rombouts, and L. Weyten, "An unconstrained architecture for systematic design of higher order $\Sigma\Delta$ force-feedback loops," *Circuits and Systems I: Regular Papers, IEEE Transactions on*, vol. 55, no. 6, pp. 1601 – 1614, Jul. 2008.

[6] J. Luo, H. Ding, and M. Kraft, "A new design methodology for electromechanical Sigma- Delta-modulators," in *IEEE NEMS'09.*, Shenzhen, CN, Jan. 2009, pp. 664–668.

[7] G. Bajdechi, O. Gielen and J. Huijsing, "Systematic design exploration of delta-sigma adcs," *Circuits and Systems I: Regular Papers, IEEE Transactions on*, vol. 51, no. 1, pp. 86 – 95, Jan. 2004.

[8] A. Hua Tang Doboli, "High-level synthesis of $\Sigma\Delta$ modulator topologies optimized for complexity, sensitivity, and power consumption," *Computer-Aided Design of Integrated Circuits and Systems, IEEE Transactions on*, vol. 25, no. 3, pp. 597 – 607, Mar. 2006.

[9] A. Marques, V. Peluso, M. Steyaert, and W. Sansen, "Optimal parameters for $\Sigma\Delta$ modulators topologies," *IEEE Trans. Circuits Syst. II,*, vol. 45, no. 9, p. 1232C1241, Sep. 1998.

[10] Y.-H. A. Ho, H.-K. Kwan, N. Wong, and K.-L. Ho, "Designing globally optimal delta-sigma modulator topologies via signomial programming," *International Journal of Circuit Theory and Application*, vol. 37, no. 23, pp. 453–472, Apr. 2009.

[11] R. Schaumann, M. Ghausi, and K. Laker, *Design of analog filters: passive, active RC and switched capacitor*. Upper Saddle River, New Jersey: Prentice-Hall Series in Electrical and Computer engineering, 1990.

[12] R. Schreier, "An empirical study of high-order single-bit delta-sigma modulators," *Circuits and Systems II: Analog and Digital Signal Processing, IEEE Transactions on*, vol. 40, no. 8, pp. 461–466, Aug 1993.

[13] G. Bourdopoulos, A. Pnevmatikakis, V. Anastassopoulos, and T. Deliyannis, *Delta–Sigma Modulators: Modeling, Design and Applications*. Imperial College Press, 2003.

[14] S. Ardalan and J. Paulos, "An analysis of nonlinear behavior in Delta-Sigma modulators," *IEEE Trans. Circ. Syst.–I*, vol. CAS-34, no. 6, pp. 593–603, Jun 1987.

[15] O. Bajdechi, J. Huijsing, and G. Gielen, "Fast exploration of $\delta\sigma$ ADC design space," in *Circuits and Systems, 2002. ISCAS 2002. IEEE International Symposium on*, vol. 2, Phoenix-Scottsdale, AZ, May. 2002, pp. 49–52.

[16] Y. Dong, M. Kraft, C. Gollasch, and W. Redman-White, "A high performance accelerometer with a fifth-order $\Sigma\Delta$ modulator," *J. Micromechan. Microeng.*, vol. 15, no. 7, pp. 22–29, Jul. 2005.

[17] Y. Dong, M. Kraft, and W. Redman-White, "High order noise-shaping filters for high-performance micromachined accelerometers," *IEEE Trans. Instr. Meas.*, vol. 56, no. 5, pp. 1666–1674, Oct. 2007.

[18] ——, "Force feedback linearization for higher-order electromechanical Sigma–Delta modulators," *J. Micromechan. Microeng.*, vol. 16, pp. S54 –S60, May. 2006.

[19] S. Mitra, *Digital Signal Processing: A Computer-Based Approach*. New York, McGraw-Hill, 1998.

[20] Y. Dong, M. Kraft, and W. Redman-White, "Micromachined vibratory gyroscopes controlled by a high-order bandpass Sigma-Delta modulator," *IEEE Sensors Journal*, vol. 7, no. 1, pp. 59 – 69, Jan. 2006.

[21] O. Shoaei, "Continuous-time Delta-Sigma a/d converters for high speed applications," Ph.D. dissertation, Department of Electronics, Carleton University, Ottawa, CAN, 1995.

[22] J. Cherry and W. Snelgrove, "Excess loop delay in continuous-time Delta-Sigma modulators," *IEEE Trans. Circuits Syst. II,*, vol. 44, no. 4, pp. 376–389, Apr. 1999.